Proc. 2nd Int. Symp. on Turbulence and Shear Flow Phenomena, June, 2001, Stockholm, Vol. 3, pp. 17-22

Effect of nonlinear interaction on feedback control of wall turbulence

Kaoru Iwamoto, Yuji Suzuki, Nobuhide Kasagi

Department of Mechanical Engineering, The University of Tokyo
Hongo, Bunkyo-Ku, Tokyo 113-8656, Japan
iwamoto@thtlab.t.u-tokyo.ac.jp

ABSTRACT

Direct numerical simulation of turbulent channel flow at $Re_\tau = 110 \sim 650$ was made in order to evaluate feedback control algorithms for reducing skin friction. The energy efficiency of the *v*-control and suboptimal control is deteriorated with increasing the Reynolds number, but it becomes almost constant above $Re_\tau = 300$. It is found through the Karhunen-Loeve decomposition of the turbulent fluctuations that the structures having large contribution to the turbulent kinetic energy are of large scale, whilst the structures having large contribution to the wall shear stress fluctuation are scaled with viscous units and accompanied with the quasi-streamwise vortices near the wall. The KL modes are divided into groups depending on the wall elevation of the structures, and the nonlinear interaction between those structures are examined. It is indicated that the interaction effect is larger at higher Reynolds numbers, but the near-wall vortices are not much affected by the interaction with the large-scale outer structures.

INTRODUCTION

From a viewpoint of saving energy and protecting the environment, it is strongly desired to develop efficient turbulence control techniques for drag reduction and/or heat transfer augmentation. Among various methodologies, active feedback control scheme attracts much attention because of its large control effect with small power input (Moin & Bewley, 1994; Gad-el-Hak, 1996; Kasagi, 1998). Choi *et al.* (1994) employed local blowing/suction on the wall based on the wall-normal velocity fluctuation in the buffer layer, and they obtained about 25% drag reduction in their direct numerical simulation (DNS) of turbulent channel flow. Bewley *et al.* (1993) applied a suboptimal control scheme (Choi *et al.,* 1993) to turbulent channel flow, and obtained about 17% drag reduction. Recently, Lee *et al.* (1998) proposed a new suboptimal control algorithm based on the linearized Navier-Stokes equation, and they obtained a simple analytical form for the control input based on the wall variables.

However, the Reynolds number assumed in most previous studies was about $Re_\tau = 100$, where significant low-Reynolds-number effects must exist. Thus, assessment of the control scheme at higher Reynolds numbers is mandatory.

The final goal of the present study is to develop a control algorithm applicable to real turbulent flows, especially high Reynolds number flows. In the present study, existing control algorithms for reducing skin friction are evaluated by using DNSs of turbulent channel flow at low-to-moderate Reynolds numbers. The contribution of coherent structures to the wall shear stress and nonlinear interactions between them are also examined through flow visualization and Karhunen-Loeve decomposition.

NUMERICAL METHOD AND CONTROL ALGORITHM

The numerical method used in the present study is almost the same as that of Kim *et al.* (1987); a pseudo-spectral method with Fourier series was employed in the streamwise (x) and spanwise (z) directions, while a Chebyshev polynomial expansion was used in the wall-normal (y) direction. A fourth-order Runge-Kutta scheme and a second-order Crank-Nicolson scheme are used for time discretization of the nonlinear terms and the viscous terms, respectively. The computational parameters are summarized in Table 1. The Reynolds number Re_τ based on the wall friction velocity u_τ and the channel half-width δ is chosen as 110, 150, 300, 400, and 650. The flow rate was kept constant at each Reynolds number. Although it is not shown here, turbulence statistics of the present computations for plane channel flow are in good agreement with the DNS data of Moser *et al*. (1999). Hereafter, u, v, and w denote the velocity components in the x, y, and z directions, respectively. Superscript + represents quantities non-dimensionalized with u_τ and the kinematic viscosity ν.

In order to evaluate the efficiency of the existing control algorithms at various Reynolds numbers, *v*-control scheme (Choi *et al.,* 1994) and the suboptimal control (Lee *et al.,* 1998) are adopted. The control input is local suction/blowing at the wall. The control input for the *v*-control is given by,

$$v_{v-control} = -\alpha v_{y^+=10} \,. \qquad (1)$$

For the suboptimal control scheme, the square of the wall-normal gradient of spanwise velocity is included in the cost function, and this leads to the control input:

$$\hat{v}_{suboptimal} = \alpha \frac{ik_z}{k} \left. \frac{\widehat{\partial w}}{\partial y} \right|_{wall} , \; k = \sqrt{k_x^2 + k_z^2} \,, \qquad (2)$$

where ^ denotes the Fourier coefficient. In Eq. (2), k_x

and k_z denote wavenumbers in the x- and z-directions, respectively. The positive constant α is chosen in such a way that the control energy is 0.05 ~ 0.4% of the pumping power. A fully developed flow field is used as the initial condition.

COHERENT STRUCTURE OF PLANE CHANNEL FLOW

Up to now, various Reynolds number effects in wall turbulence are reported. George & Castillo (1997) and Barenblatt *et al*. (1997) suggest that the overlap region between inner and outer scalings in wall-bounded turbulence may yield a power law rather than a log law at very high Reynolds number. Moser *et al*. (1999) made DNSs of fully developed turbulent channel flow at Re_τ = 180 ~ 590. They found that the wall-limiting behavior of the rms velocity fluctuation strongly depends on the Reynolds number, but obvious low-Reynolds-number effects are absent at $Re_\tau > 395$.

In this chapter, the effect of Reynolds number on the coherent structure in a low-to-moderate Reynolds number range is examined by visualizing instantaneous flow fields.

Near-wall coherent structures play an important role in transport mechanisms in wall turbulence (e.g., Robinson, 1991; Kasagi *et al*., 1995). The wall shear stress is also associated with the near-wall streamwise vortices (Kravchenko *et al*., 1993). It is indicated by a number of studies that the near-wall structures are self-sustained through regeneration mechanisms (Brooke & Hanratty, 1993; Hamilton *et al*., 1995; Jeong *et al*., 1997). Jimenez & Pinelli (1999) claim that the near-wall region below $y^+ \simeq 60$ is self-sustaining and does not depend on the outer flow.

Figure 1 shows a plane view (x - z) of an instantaneous flow field, in which the near-wall vortical structures identified with 3-D contours of the second invariant of the deformation tensor ($Q^+ < -0.02$) as well as the distribution of the wall shear stress are visualized. When $Re_\tau = 110$, most vortices are located near the wall and aligned in the streamwise direction. The area of large skin friction is accompanied with the near-wall streamwise vortices. Although it is not shown here, the production of turbulent energy is large on both sides of the streamwise vortices, where the ejection/sweep events occur (Robinson, 1991; Kasagi *et al*., 1995). It is found that this is also the case for Re_τ = 650; the near-wall streamwise vortices are responsible for the wall shear stress and the turbulent production near the wall.

Figure 2 shows a plane view (x - z) of vortical structures at $Re_\tau = 650$. Unlike at $Re_\tau = 110$, vortices seem different in their scales and shapes. It is found that the vortices form clusters at some regions (e.g., area A in Fig. 2), leaving some regions without vortices (e.g., area B in Fig. 2). These densely-populated vortices are in accordance with the packets of hairpin vortices observed by Adrian *et al*. (2000).

Table 1. Computational parameters for the DNS of turbulent channel flow. Δy_c^+ is the y interval in the center of the channel.

Re_τ	L_x	L_z	N_x, N_y, N_z	Δx^+	Δy_c^+	Δz^+
110	5π	2π	48, 64, 48	36.0	5.40	14.4
150	2.5π	π	64, 96, 64	18.4	4.91	7.36
300	2.5π	π	128, 192, 128	18.4	4.91	7.36
400	2.5π	π	192, 256, 192	16.4	4.91	6.54
650	2.5π	π	288, 256, 288	17.7	7.98	7.09

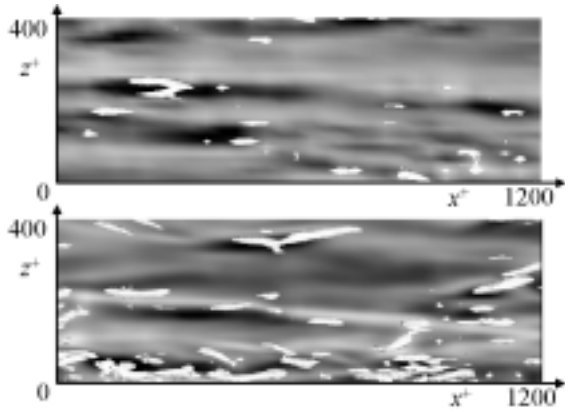

Figure 1 Plane view of near-wall coherent structures. White, the second invariant of the deformation tensor ($Q^+ < -0.02$) below $y^+ = 20$; Contours of the wall shear rate $\tau_w'^+$, Gray to Black, -1.0 to 1.0. (a)Re_τ = 110, (b)Re_τ = 650.

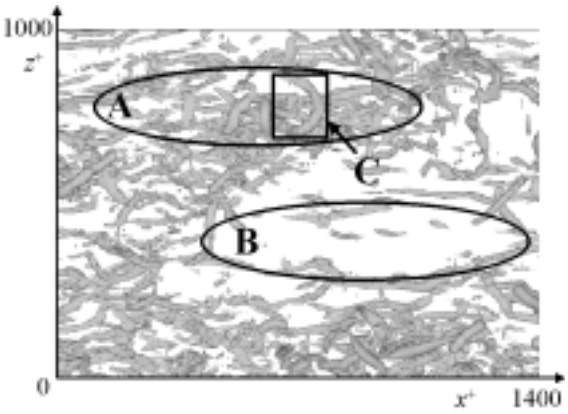

Figure 2 Plane view of vortical structures at Re_τ = 650. Gray, $Q^+ < -0.02$.

Figure 3 shows a magnified 3-D view of a hairpin vortex (area C in Fig. 2). In addition to the sides of the near-wall streamwise vortices, the region of large turbulent energy production P^+ is also located on the neck of the vortex away from the wall at this higher Reynolds number (Robinson, 1991).

When $Re_\tau = 110$, the cumulative production rate of turbulent kinetic energy at $y^+ < 50$ reaches 90% of the total production (not shown here). On the other hand, the same region covers only 60% of the total production when $Re_\tau = 650$. Therefore, as far as the turbulent energy production is concerned, the structures in somewhat outer layer should also play an important role.

REYNOLDS NUMBER EFFECT ON FEEDBACK CONTROL

Figure 4 shows the drag reduction rate under *v*-control versus the constant of α in Eq. (1). Since the flow rate is kept constant, the drag reduction rate is equivalent with the ratio of the pumping power saved to the pumping power. The present result at $Re_\tau = 110$ is in good agreement with the DNS data of Choi *et al*. (1994); the drag reduction of about 20% is achieved with $\alpha = 1$. The drag reduction rate is increased with increasing α at each Reynolds number. As a whole, the drag reduction rate decreases as the Reynolds number is increased and eventually seems to reach some asymptotic values.

Figure 5 shows the drag reduction rate versus the power input ratio, which is the blowing/suction work divided by the pumping power of driving fluid in the channel. Unlike in Fig. 4, when the Reynolds number is increased while keeping the power input ratio constant, the control effect is decreased drastically. However, the drag reduction rate eventually becomes insensitive to the Reynolds number at $Re_\tau > 300$. Note that two different control algorithms exhibit a similar trend, but in general, the suboptimal control requires less power input than the *v*-control scheme for the same amount of the drag reduction.

Therefore, although the existing control algorithms, of which major control target is the near-wall streamwise vortices, are effective at all Reynolds numbers tested, the energy efficiency is deteriorated with increasing the Reynolds number. Thus, further study of algorithms is required for high-Reynolds-number flow control. It is noted that the present result for feedback control is in accordance with the findings of Moser *et al*. (1999) that obvious low-Reynolds-number effects are absent at $Re_\tau > 300 \sim 400$. Therefore, it is expected that some clue for more advanced control scheme can be obtained by comparing the underlying flow mechanisms between $Re_\tau \sim 100$ and 300, although $Re_\tau = 300$ is not to be considered as a high Reynolds number.

INTERACTIONS BETWEEN COHERENT STRUCTURES

In order to analyze the contribution of coherent structures to transport mechanisms, interactions between coherent structures are investigated by using the Karhunen-Loeve decomposition (Lumley, 1970).

Karhunen-Loeve Decomposition

The Karhunen-Loeve decomposition is based on the decomposition of the fluctuating velocity field into a sum of mutually orthogonal eigenfunctions φ_i of the two-point correlation tensor κ_{ij} (Lumley, 1981; Moin & Moser, 1989; Sirovich *et al*., 1990).

$$\int_{-h}^{h} \kappa_{ij}(y, y', m, n)\varphi_j(y', m, n)dy' = \lambda(m, n)\varphi_i(y), \quad i, j = 1 - 3, \tag{3}$$

where m and n denote wavenumbers in the x and z directions, respectively, while λ denotes the eigenvalue. The number of eigenvalue for each wavenumber index pair (m, n) is three times of N_2, which is the number of grid points in the y direction. Each eigenfunction is specified with a triplet $\mathbf{k} = (m, n, q)$ (Webber *et al*., 1997). The three dimensional eigenfuction is a complex valued vector field, which can be written as:

$$\boldsymbol{\phi}^{\mathbf{k}}(x, y, z) = \boldsymbol{\varphi}^{\mathbf{k}}(y, m, n)e^{2\pi i(mx/L_1 + nz/L_3)}. \tag{4}$$

Any velocity field is decomposed as a linear superposition of the eigenfucntions as follows:

$$\boldsymbol{u}(\boldsymbol{x}, t) = \sum_{\mathbf{k}} a^{\mathbf{k}}(t)\boldsymbol{\phi}^{\mathbf{k}}(\boldsymbol{x}). \tag{5}$$

Note that the eigenvalues $\lambda^{\mathbf{k}}$ represent the energy in each KL mode (Lumley, 1981), so that eigenfunctions can be sorted according to its contribution to the turbulent energy.

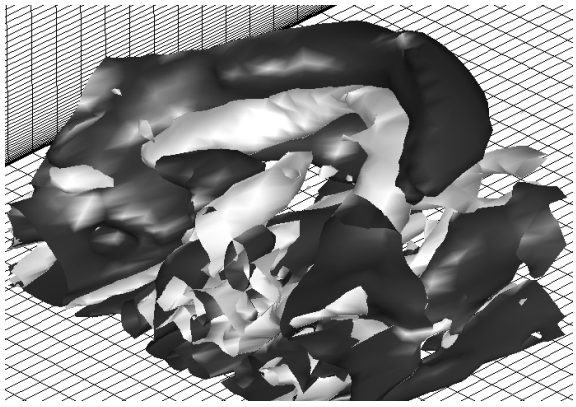

Figure 3 Vortical structures and turbulent energy production at $Re_\tau = 650$ (area C in Fig. 2). Gray, $Q^+ < -0.02$; Black, production of the turbulent kinetic energy ($P^+ > 0.1$).

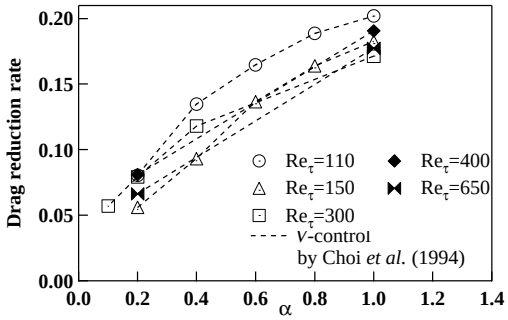

Figure 4 Drag reduction rate versus the constant of α in Eq. (1).

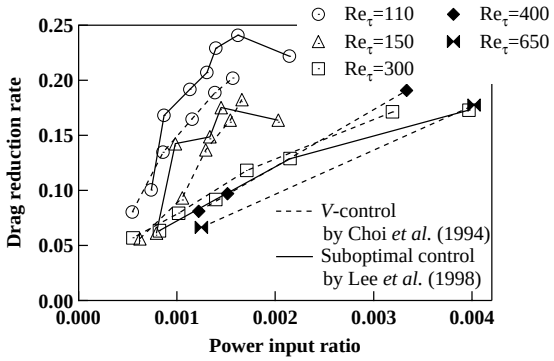

Figure 5 Drag reduction rate versus power input ratio.

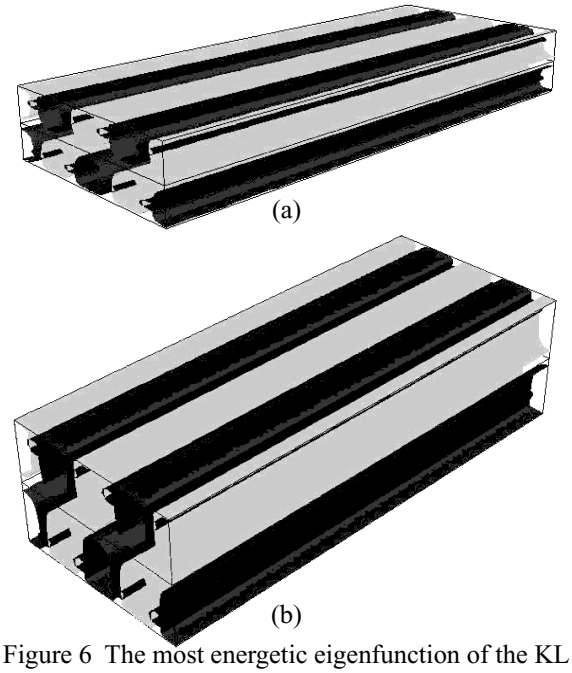

Figure 6 The most energetic eigenfunction of the KL decomposition. Isosurfaces of u'^{+} and the second invariant of the deformation tensor Q^{+} are shown. White, $u'^{+} > 0.15$; Gray, $u'^{+} < -015$; Black, $Q^{+} < 0$. (a)Re_τ = 110, (b)Re_τ = 300.

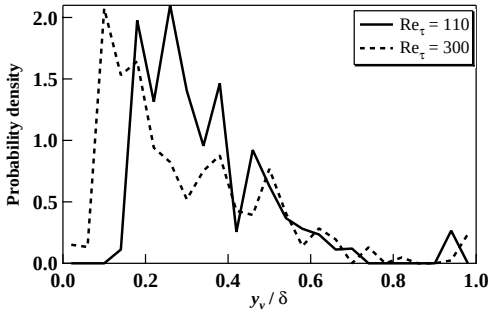

Figure 7 Probability density function of y_v of top 50% eigenfunctions in global coordinates.

Turbulent Kinetic Energy of KL Modes

Figure 6 shows the most energetic eigenfunction of the KL decomposition for Re_τ = 110 and 300. For both Reynolds numbers, large-scale low and high speed regions and large vortices homogeneous in the streamwise direction are observed. This fact is in accordance with the result of Webber *et al*. (1997) for the minimal channel flow (Jimenez & Moin, 1991) at Re_τ = 136. The wall elevation of the center of the vortices y_v^+ is about 50 at Re_τ = 110 and about 120 at Re_τ = 300, respectively.

Figure 7 shows the probability density function of the location of a vortex y_v, for eigenfunctions contributing to 50% cumulative energy. It is found that y_v is scaled with δ except the near wall region and that the average value of y_v/δ is about 0.3 for both Reynolds numbers. Therefore, the structures having large contribution to the turbulent kinetic energy are likely to be the large streamwise vortices, which can be scaled with the channel half-width.

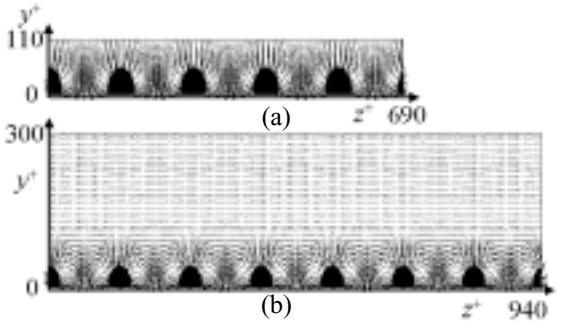

Figure 8 Eigenfunction of the KL decomposition making the largest contribution to the rms value of the wall shear stress. Velocity vectors in the cross-stream plane and contours of the streamwise velocity fluctuation u'^{+} are shown. Gray, $u'^{+} > 0.15$; Black, $u'^{+} < -015$. (a)Re_τ = 110, (c)Re_τ = 300.

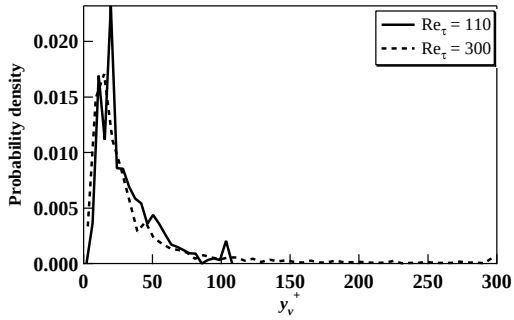

Figure 9 Probability density function of y_v for top 50% eigenfunctions for the rms value of the wall shear stress in wall coordinates.

Contribution of KL Modes to Skin Friction

In order to evaluate the contribution of KL modes to the skin friction, the rms value of the wall shear stress $\tau_{w,rms}$ of each KL mode is computed. Figure 8 shows the eigenfunction having the largest contribution to $\tau_{w,rms}$ for Re_τ = 110 and 300 in the cross-stream plane. For both Reynolds numbers, low and high speed streaks and near-wall streamwise vortices are observed. The eigenfunction at Re_τ = 110 is homogeneous in the streamwise directions, and y_v^+ is about 34. The spanwise spacing of the structure Δz^+ is about 138. On the other hand, the eigenfunction at Re_τ = 300 has one wave number in the streamwise direction. These structures are tilted away from the wall by a shallow angle, and y_v^+ and Δz^+ are about 31 and 134, respectively.

Figure 9 shows the probability density function of y_v for eigenfunctions making 50% contribution to the cumulative rms value of the wall shear stress. Unlike the vortices accompanied with the most energetic structures, y_v is not scaled with δ, but scaled with the wall unit. The average value of y_v^+ is about 30 at both Reynolds numbers. Therefore, the structures having large contribution to the fluctuation of skin friction are associated with the near-wall streamwise vortices scaled with wall units. The present finding using KL decomposition is in qualitative accordance with the visualization result shown in Fig. 1 and the previous studies (Robinson, 1991; Kravchenko *et al*., 1993).

Interactions between KL Modes

By using KL decomposition, the transport equation of the turbulent energy for each KL mode can be calculated. However, it requires huge computational load. Thus, in this study, the KL modes are divided into groups depending on y_v, and the interaction between these groups are examined. The structure $\boldsymbol{u}_\alpha$ represents the superposition of the KL modes, of which y_v is in between $y_{v\alpha}$ - Δy_v and $y_{v\alpha}$:

$$\boldsymbol{u}_\alpha(\boldsymbol{x},t) \equiv \sum_{y_{v\alpha}-\Delta y_v<y_v<y_{v\alpha}} a^{\mathbf{k}}(t)\boldsymbol{\phi}^{\mathbf{k}}(\boldsymbol{x}), \qquad (6)$$

where $\Delta y_v^+ = 10$ and 15 respectively for $\mathrm{Re}_\tau = 110$ and 300. The energy equation of $\boldsymbol{u}_\alpha$ leads to,

$$\begin{aligned} 0 = &\left\langle \sum_{y_{v\beta}} \left(-u_{1\alpha}^+ u_{2\beta}^+\right)\partial U^+/\partial y^+ \right\rangle \\ &+\left\langle \sum_{y_{v\beta}} \sum_{y_{v\gamma}} \left(-u_{i\alpha}^+ u_{j\beta}^+\right)\partial u_{i\gamma}^+/\partial x_j^+ \right\rangle \\ &+\left\langle -u_{i\alpha}^+ \partial p^+/\partial x_i^+ \right\rangle \\ &+\left\langle 1/\mathrm{Re}_\tau \sum_{y_{v\beta}} u_{i\alpha}^+ \partial^2 u_{i\beta}^+/\partial x_j^+ \partial x_j^+ \right\rangle, \end{aligned} \qquad (7)$$

where the first, second, third and fourth terms of RHS correspond to the production, nonlinear interaction, pressure and viscous terms, respectively. The bracket $\langle\ \rangle$ denotes the time-space average.

It is found that the production term has non-zero value only when $y_{v\alpha} = y_{v\beta}$ for both Reynolds numbers (not shown). Thus, the turbulent kinetic energy of the structure $\boldsymbol{u}_\alpha$ is generated through the Reynolds shear product with the same structure $\boldsymbol{u}_\alpha$. The production has a large peak at $y_{v\alpha}^+ = 30$, which is in accordance with the previous studies showing that turbulence producing event is located on the sides of near-wall vortices (Kasagi *et al*., 1995).

Figure 10 shows the nonlinear interaction term of the structures for $\mathrm{Re}_\tau = 110$. For $\boldsymbol{u}_{30}$ ($y_{v\alpha}^+ = 30$), two negative peaks are observed at ($y_{v\beta}^+$, $y_{v\gamma}^+$) = (30, 20) and (30, 60). On the other hand, $\boldsymbol{u}_{20}$ ($y_{v\alpha}^+ = 20$) and $\boldsymbol{u}_{60}$ ($y_{v\alpha}^+ = 60$) have a positive peak at ($y_{v\beta}^+$, $y_{v\gamma}^+$) = (30, 30) as shown in Figs. 10(a) and (c). Thus, the structure of $\boldsymbol{u}_{30}$ loses the turbulent kinetic energy through the nonlinear interaction, and the energy is transferred to the structures of $\boldsymbol{u}_{20}$ and $\boldsymbol{u}_{60}$. Therefore, the nonlinear interaction for $\mathrm{Re}_\tau = 110$ is similar with the turbulent diffusion, in which the turbulent energy is transferred from the buffer region to the viscous sublayer and the outer layer.

Figure 11 shows contours of nonlinear interaction term for $\mathrm{Re}_\tau = 300$. It has a negative peak at ($y_{v\beta}^+$, $y_{v\gamma}^+$) = (30, 15) for $y_{v\alpha}^+ = 30$, and a positive peak at around ($y_{v\beta}^+$, $y_{v\gamma}^+$) = (30, 30) for $y_{v\alpha}^+ = 15$. Thus, the similar energy transfer mechanism from $\boldsymbol{u}_{30}$ to the viscous sublayer is present at the higher Reynolds number. On the other hand, the nonlinear interaction ($y_{v\beta}^+$, $y_{v\gamma}^+$) = (60, 60) at $y_{v\alpha}^+ = 30$ is positive value, while the interaction at $y_{v\alpha}^+ = 60$ is negative at around ($y_{v\beta}^+$, $y_{v\gamma}^+$) = (60, 30). Therefore, at $\mathrm{Re}_\tau = 300$, the structure of $\boldsymbol{u}_{30}$, which makes the largest contribution to the skin friction, gains energy from the structure somewhat away from the wall through the nonlinear interaction.

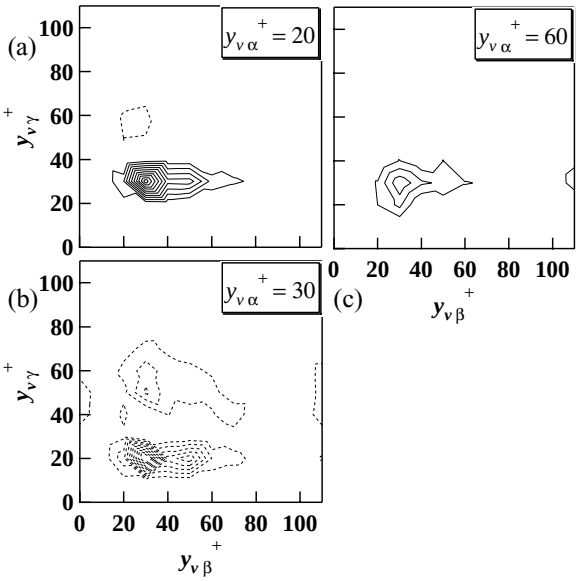

Figure 10 Contours of the nonlinear interaction term between KL modes for $\mathrm{Re}_\tau = 110$. The contour levels range from -0.004 to 0.004 by increments of 0.0004. Negative contours are dotted. (a)$y_{v\alpha}^+ = 20$, (b)$y_{v\alpha}^+ = 30$, (c)$y_{v\alpha}^+ = 60$.

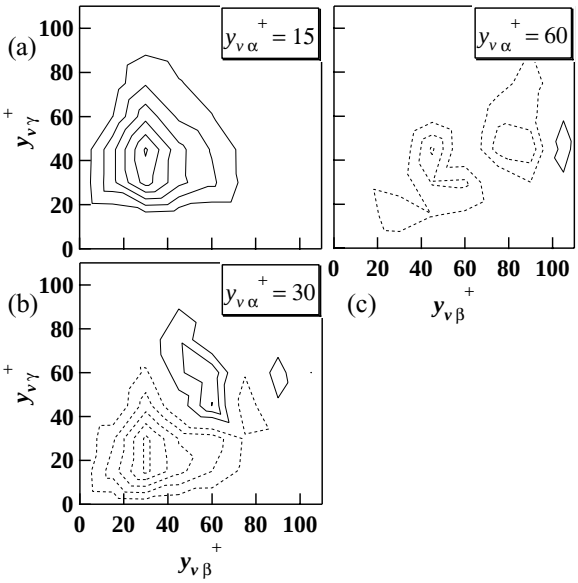

Figure 11 Contours of the nonlinear interaction term between KL modes for $\mathrm{Re}_\tau = 300$. The contour levels range from -0.004 to 0.004 by increments of 0.0004. Negative contours are dotted. (a)$y_{v\alpha}^+ = 15$, (b)$y_{v\alpha}^+ = 30$, (c)$y_{v\alpha}^+ = 60$.

It is noted that the mean value of the nonlinear interaction for $y_{v\alpha}^+ = 30$ is small at $y_v^+ > 100$ (Fig. 11(b)), and the rms value based on only temporal averaging of this interaction is also small at $y_v^+ > 100$ (not shown here). Therefore, $\boldsymbol{u}_{30}$ is free from the nonlinear interaction from the large-scale outer structures. More detailed analysis using KL modes is required in order to elucidate the dynamics of the near-wall structures and their mutual interaction.

TOWARD EFFICIENT FEEDBACK CONTROL ALGORITHM

Although the nonlinear interaction is the central mechanism in isotropic turbulence, the linear process is also considered to be important for wall turbulence. Lee *et al*. (1990) found that the formation of streaky structures is essentially linear mechanism. Kim & Lim (2000) show that the linear coupling term in the wall-normal vorticity equation is crucial for turbulence sustenance. The importance of linear process for wall turbulence is also supported by the fact that the direct suppression of the near-wall vortices responsible for the wall-skin friction leads to large drag reduction. Moreover, the efficient suboptimal control algorithm proposed by Lee *et al*. (1998) is based on linearized Navier-Stokes equations.

However, when the Reynolds number is increased, the contribution of outer structures to turbulent energy is also increased. Thus, the nonlinear interaction between near-wall and larger structures might play important role in the self-sustaining mechanism of wall turbulence.

It is shown in the present KL decomposition that the effect of the nonlinear interaction is actually increased at a higher Reynolds number. However, the interaction with the near-wall vortices is confined in relatively near-wall region, $y^+ < 100$. The increase of the nonlinear mechanism in dynamics of turbulence is in accordance with the visualization of vortices presently made, where the clusters of vortices are formed in higher Reynolds number. Moreover, the efficiency of existing feedback control algorithms is decreased with increasing Reynolds number. Therefore, nonlinear interaction near the wall should also be taken into account.

CONCLUSIONS

Direct numerical simulation of turbulent channel flow was made in order to evaluate the performance of feedback control algorithms. KL decomposition is applied to examine the effect of interaction between near-wall and outer structures quantitatively. The following conclusions are derived:

1) The energy efficiency of *v*-control and the suboptimal control is deteriorated with increasing the Reynolds number.
2) The KL modes, which make large contribution to the wall shear stress fluctuation, are accompanied with near-wall streamwise vortices and streaky structures, which are scaled with wall units.
3) The effect of nonlinear interaction between KL modes are increased at a higher Reynolds number, $Re_\tau = 300$. However, the interaction with the near-wall vortices is confined in relatively near-wall region of $y^+ < 100$.

ACKNOWLEDGMENTS

This work was partially supported through the Project for Organized Research Combination System, and also through the Grant-in-Aid for Science Research on Priority Areas (B) by the Ministry of Education, Culture, Sports, Science and Technology of Japan (MEXT).

REFERENCES

Adrian, R. J., Meinhart, C. D., and Tomkins, C. D., 2000, *J. Fluid Mech.* **422**, 1.

Bewley, T., Choi, H., Temam, R., and Moin, P., 1993, *CTR Annual Research Briefs* 3.

Brooke, J. W., and Hanratty, T. J., 1993, *Phys. Fluids* A **5**, 1011.

Barenblatt, G. I., Chorin, A., and Prostokishin, V. M., 1997, *Appl. Mech. Rev.* **50**, 413.

Choi, H., Temam, R., Moin. P., and Kim, J., 1993, *J. Fluid Mech.* **253**, 509.

Choi, H., Moin, P., and Kim, J., 1994, *J. Fluid Mech.* **262**, 75.

Gad-el-Hak, M., 1996, *Appl. Mech. Rev.* **49**, 7, 365.

George, W. D., and Castillo, L., 1997, *Appl. Mech. Rev.* **50**, 689.

Hamilton, J. M., Kim, J., and Waleffe F., 1995, *J. Fluid Mech.* **287**, 317.

Jimenez, J., and Moin, P., 1991, *J. Fluid Mech.* **225**, 213.

Jimenez, J., and Pinelli, A., 1999, *J. Fluid Mech.* **389**, 335.

Jeong, J., Hussain, F., Schoppa, W., and Kim, J., 1997, *J. Fluid Mech.* **332**, 185.

Kasagi, N., Sumitani, Y., Suzuki, Y., and Iida, O., 1995, *Int. J. Heat & Fluid Flow* **16**, 2.

Kasagi, N., 1998, *Int. J. Heat & Fluid flow* **19**, 125.

Kim, J., and Lim, J., 2000, *Phys. Fluids* **12**, 8, 1885.

Kim, J., Moin, P., and Moser, R., 1987, *J. Fluid Mech.* **177**, 133.

Kravchenko, A. G., Choi, H., and Moin, P., 1993, *Phys. Fluids* A **5**, 12, 3307.

Lee, C., Kim, J., and Choi, H., 1998, *J. Fluid. Mech.* **358**, 245.

Lee, M. J., Kim, J., and Moin, P., 1990, *J. Fluid Mech.* **216**, 561.

Lumley, J. L., 1970, *Stochastic tools in turbulence*. Academic.

Lumley, J. L., 1981, *Transition and Turbulence* (ed. R. E. Meyer), 215, Academic.

Moin, P., and Moser, R., 1989, *J. Fluid Mech.* **200**, 471.

Moin, P., and Bewley, T., 1994, *Appl. Mech. Rev.* **47**, S3.

Moser, R. D., Kim, J., and Mansour, N. N., 1999, *Phys. Fluids* **11**, 4, 943.

Robinson, S. K., 1991, *NASA TM* 103859.

Sirovich, L., Ball, K. S., and Keefe, L. R., 1990, *Phys. Fluids* A **2**, 2217.

Webber, G. A., Handler, R. A., and Sirovich, L., 1997, *Phys. Fluids* **9**, 1054.